Proceedings World Geothermal Congress 2015
Melbourne, Australia, 19-25 April 2015

Kinetics of Galvanic Corrosion of Carbon Steel to Arsenic and Antimony Couples

Keith A. Lichti[1], Lily Wallis[1], Monika Ko[1] and John Kennedy[2]

[1]Quest Integrity Group, PO Box 38096, Lower Hutt, New Zealand

[2]National Isotope Centre, GNS Science, PO Box 31312, Lower Hutt, New Zealand

k.lichti@questintegrity.com, m.ko@questintegrity.com, j.kennedy@gns.cri.nz

Keywords: Galvanic Corrosion, Arsenic, Antimony, Carbon Steel, Geothermal, Brine

ABSTRACT

Carbon steel has been observed to experience accelerated corrosion in pH adjusted geothermal brines. The damage mechanisms observed in service have included; localised under-film corrosion, galvanic corrosion and erosion corrosion. The magnitude of these differing damage mechanisms has been difficult to deduce from the in-service history of corrosion and a laboratory study has been initiated to better quantify the effects of pH, temperature and chloride content on localised corrosion under heavy metal scales and galvanic corrosion. The study of antimony was progressed previously as this material was readily available in solid form. Arsenic was not readily available and a series of tests using vapour deposited arsenic layers on carbon steel was initiated. This paper describes progress in the study of the corrosion properties of galvanic couples of carbon steel to antimony and carbon steel to arsenic in laboratory solutions at temperatures up to 80°C.

1. INTRODUCTION

Geothermal energy is an economically reliable, safe and environmentally friendly alternative energy source which accounts for about 13% of New Zealand's national energy production. A limited number of service conditions have been observed to cause undesirable corrosion degradation of carbon steel facilities. This is predominantly due to corrosive chemicals in the geothermal fluids, specifically chlorides, hydrogen sulphide and carbon dioxide (Shannon, 1977, Lichti, 2006). Nevertheless, for most of the common engineering alloys in air-free geothermal fluids, the corrosion rates are sufficiently low to ensure adequate service life.

Of recent interest are the effects of heavy metal deposition on the materials performance of carbon steels in geothermal brines. Geothermal fluids in many cases may contain traces of heavy metals, such as gold, silver, thallium, arsenic, antimony and copper to mention a few. Under certain conditions, electrochemical reduction of these heavy metal species, particularly of antimony, antimony/silver and arsenic can result in deposited scales forming on freely corroding carbon steel. Precipitation of unwanted scales and corrosion in plant and piping causes major engineering challenges, leading to reduced efficiencies, plant shutdowns, costly scale removal and limits on downstream use of fluids. Apart from that, these scales, formed in conjunction with oxidation of iron have subsequently been associated with localised galvanic corrosion, under scale pitting and erosion corrosion of the underlying carbon steel (Lichti and Brown, 2013, Amend and Yee, 2013). The conditions leading to corrosion are poorly understood.

The fluids of primary interest are mildly acidic brines that appear to be the main drivers for the electrochemical reduction and for the subsequent galvanic corrosion. Under low pH conditions, both in two-phase fluids and in brines, arsenic and antimony have been observed to precipitate as metallic materials. Acid well fluids are not utilized in New Zealand geothermal production, however, acid process conditions can be encountered either through deliberate modification of the environment, for silica scale control for example or in power station circuits where the acidic geothermal gases (CO_2 and H_2S) are concentrated. The deposition occurs through oxidation and reduction reactions that are illustrated below for arsenic and antimony as proposed by (Gallup, 1992):

Oxidation of iron: $Fe \rightarrow Fe^{2+} + 2e^-$ (1)

Reduction of arsenic: $AsO^+ + 2H^+ + 3e^- \rightarrow As + H_2O$ (2)

Reduction of antimony: $SbO^+ + 2H^+ + 3e^- \rightarrow Sb + H_2O$ (3)

Silver has also been observed in the resulting heavy metal scales and indeed silver-antimony alloys are commonly seen in New Zealand geothermal power plants. The process of oxidation/reduction has been observed to show pH dependence as it appears that iron must be rapidly taken into solution and not precipitated as a protective corrosion product film for the elemental scales to form. Acidity is required for the reduction processes as seen in the above equations. Under alkali and near neutral to slightly acid conditions where iron oxides and iron sulfides are stable heavy metal precipitation is not observed (Lichti and Brown, 2013). In some cases precipitation of silicon rich scales slow the oxidation reactions required for heavy metal reduction. However, there has been no distinctive identification of the factors that control corrosion (pH, chloride content, heavy metal concentration, silica saturation index or other) and it is not known if arsenic scales or antimony scales or a mix of the two lead to accelerated corrosion.

A corrosion study of heavy metal scales coupled to carbon steel was initiated in the laboratory with pure antimony and carbon steel using a potentiostat to measure the potential differences between the two metals and at the same time measure the driving force for corrosion when these two electrodes are coupled together (Soltis and Lichti, 2012). The work presented here builds on a previously published work to include arsenic coupled to carbon steel with an objective to improve mechanistic understanding on factors and process conditions controlling the precipitation of heavy metal species and its consequences on corrosion under power station

production conditions. Thermodynamic properties of arsenic and antimony required to model the stability of arsenic, antimony and iron-arsenic compounds at high temperatures are being reviewed as part of this research programme. The work aims to increase understanding of heavy metal scaling conditions in order to set operational parameters for corrosion environment control in existing and new geothermal energy plants.

2. EXPERIMENTAL

Two different methods were used to study the galvanic effects of heavy metals/carbon steel coupling: electrochemical polarization testing and open circuit coupon exposure testing. The conditions of interest for this study are chloride solution at pH 3 and 5.4, at temperatures up to 80°C in both aerated (open to air, not deliberately bubbled with air) and oxygen-free environments. Experimental electrolyte comprised of ultra-pure water with 1000 ppm of chloride ions added in the 3.7:1 ratio of sodium and potassium chloride. The pH of the electrolyte was adjusted by the addition of small amounts of 0.05 mol.dm^{-3} solution of sulfuric acid (H_2SO_4). Oxygen-free environment was achieved by bubbling high purity nitrogen gas for one hour prior to testing and was used to shield the atmosphere during measurements. The test matrix conducted for this work is given in Table 1.

Table 1: Test Matrix – (Galvanic Corrosion Study)

Test Method	Samples		Conditions
Coupon Exposure 4 Days Test + Scratch Test	Plated coupon	Sb-CS	pH 3 and pH 5.4, 20°C, Aerated
		As-CS	pH 3 and pH 5.4, 20°C, Aerated
Electrochemistry Study Polarisation/ Evans Methods	Solid electrode	CS	pH 3: 20°C, 60°C (N_2 Purged/Aerated) pH 4.5: 20°C (N_2 Purged/Aerated) pH 5.4: 20, 60, 80°C (N_2 Purged/Aerated)
		Sb *vs.* CS	pH 3: 20°C, 60°C (N_2 Purged/Aerated) pH 4.5: 20°C (N_2 Purged/Aerated) pH 5.4: 20, 60, 80°C (N_2 Purged/Aerated)
		As *vs.* CS	pH 5.4: 20, 60, 80°C (N_2 Purged/Aerated)

2.1 Electrochemical Tests

All electrochemical measurements were obtained by using a PGZ 100 potentiostat (Radiometer Analytical) and EG&G Model 273A potentiostat (Princeton Applied Research). Measurements were conducted using a typical three-electrode electrochemical cell with a double-wall arrangement. Such a custom-made design allowed for a hydronic heating of the experimental electrolyte, with both the heating mantle (Electrothermal, UK) and the peristaltic pump (Watson-Marlow 505S, UK) located outside a Faraday cage to minimize electromagnetic interference (see Figure 1 for experimental set up).

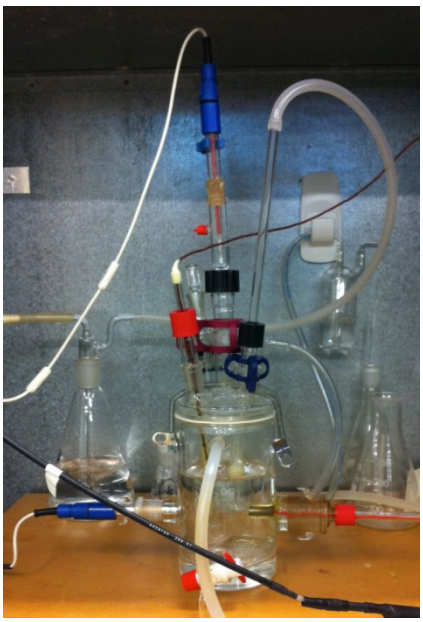

Figure 1: Photo of the experimental set up for Polarisation Experiments.

A calomel electrode with saturated KCl (SCE) was used as the reference (all potentials reported were referred to SCE) and a platinum electrode as the auxiliary. Antimony and carbon steel electrodes were prepared using rods of high purity antimony (Goodfellow Materials, England) and AISI 1018 carbon steel with a diameter of 6 mm. A copper-tin wire was soldered to one end to provide electrical connection then degreased with ethanol and cleaned with acetone. The arsenic electrode was prepared using sintered arsenic with a diameter of 10 mm and had a degree of porosity. Arsenic was attached to a metal holder by silver epoxy resin which was soldered to a copper-tin wire. The metal was mounted in K36 coating and laminating epoxy resin (Nuplex Industried Ltd. New Zealand). Electrode surfaces were ground to 1200 grit with SiC-Paper and rinsed with distilled water and cleaned with ethanol. Figure 2 displays the very porous structure of the arsenic surface. All electrodes were stored with silica desiccant when not in use.

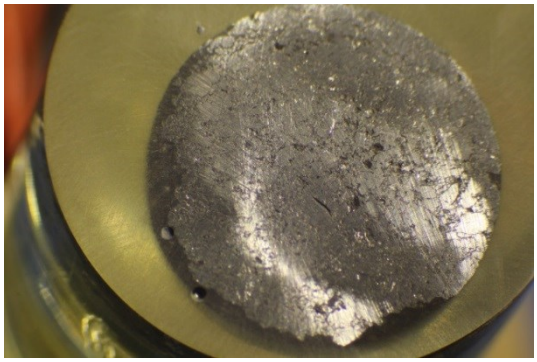

Figure 2: Photo of the surface of the arsenic electrode

2.1.1 Potentiodynamic Scans

Potentiodynamic scans were conducted after a 900 s hold at the free corrosion potential, E_{corr}, and then initiated at -500mV below the E_{corr} to +500mV above E_{corr} at a scan rate of 0.1-0.2 $mV.s^{-1}$

2.1.2 Evans Measurement

The corrosion current that was expected to take place at the mixed potential of heavy metals–carbon steel couples was measured using the Evans' experiment, where the more electronegative material (carbon steel) was used as the working electrode and the less electronegative materials (antimony and arsenic) were the auxiliary electrodes. Galvanostatic steps of 0.1-0.2µA were applied with a drift threshold of 3mV/min and a maximum step duration of 30 seconds, until a mixed potential was measured to provide the galvanic corrosion current.

2.2 Coupon Exposure Test

Open circuit coupon exposure tests were conducted in a sealed glass cell with a coupon holder which allowed for open circuit potential monitoring during the exposure period. Carbon steel coupons (AISI 1018) with a diameter of 14 mm were used as the base material for the heavy metal coated coupon exposure experiments. The carbon steel coupons were ground to a 1000 grit surface and then coated with an antimony, arsenic or iron arsenide layer using an ion beam sputtering (IBS) technique (Murmu *et al*., 2011). The sputtering process was done under high vacuum conditions of 10^{-7} mbar. The carbon steel coupons were mounted onto the catchers, which were angled at 60º to the vertical. The substrate holder and target holders were rotated in opposite directions to ensure the uniformity of the film. A Quartz thickness monitor was installed in the chamber to measure the thickness of the deposited film. The film thickness was found to be around 0.5 µm. The coupons were 'scratched' to facilitate galvanic corrosion with a large cathodic area (heavy metal coating) and a small anodic area (exposed steel surface). Unscratched coupons and plain carbon steel coupons were exposed to the same electrolyte, temperature and aeration conditions for comparison.

Coupons were exposed for periods of 4 days and upon completion of the exposure test, coupons were removed, rinsed with distilled water and dried. The dried coupons were then chemically cleaned with tri-ammonium citrate at room temperature or di-hydrogen ammonium citrate under cathodic protection at 60°C. The cleaned coupons were inspected to characterise the corrosion damage and sectioned for SEM analysis.

3. RESULTS

3.1 Electrochemical Tests

3.1.1 Free Corrosion Potential

A summary of free corrosion potential (E_{corr}) measurements of antimony, arsenic and carbon steel in varying test conditions (temperature, pH and aeration) are given in Figure 3 to Figure 5. Figure 3 shows that the E_{corr} value of antimony at pH 3 shifts to more active values with increasing temperature in the aerated solution, however, E_{corr} remained constant when exposed to de-aerated solution achieved by N_2 purging. For carbon steel at the same conditions, there were small differences for changes in aeration and temperature.

Figure 4 shows the change in potential value with pH levels. Antimony in both environments follows a similar trend, potential decreases for the pH 3 vs. pH 4.5 solution with a slight increase in potential for pH 5.4. Carbon steel also follows a similar trend however aeration has a more drastic change for pH 5.4. Figure 5 shows free corrosion potential of arsenic and carbon steel at pH 5.4 and temperatures between 20°C to 80°C. The E_{corr} of arsenic decreases with increasing temperatures and with de-aeration by N_2 purging. Aeration showed significant effect on the E_{corr} of carbon steel at 20°C, however little difference was observed at higher temperatures of 60 and 80°C, presumed due to lower oxygen solubility at higher temperatures. The free corrosion potential of carbon steel in the de-aerated solution remained more or less constant at all temperatures.

These graphs show that antimony and arsenic are less electronegative (cathodic) compared to carbon steel under all experimental conditions.

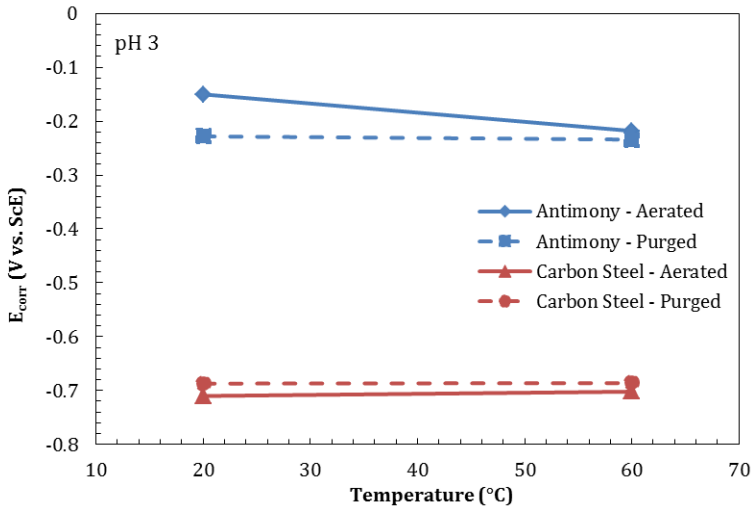

Figure 3: Free corrosion potential, E_{corr} for carbon steel and antimony (pH 3) as a function of temperature for the aerated and purged environment.

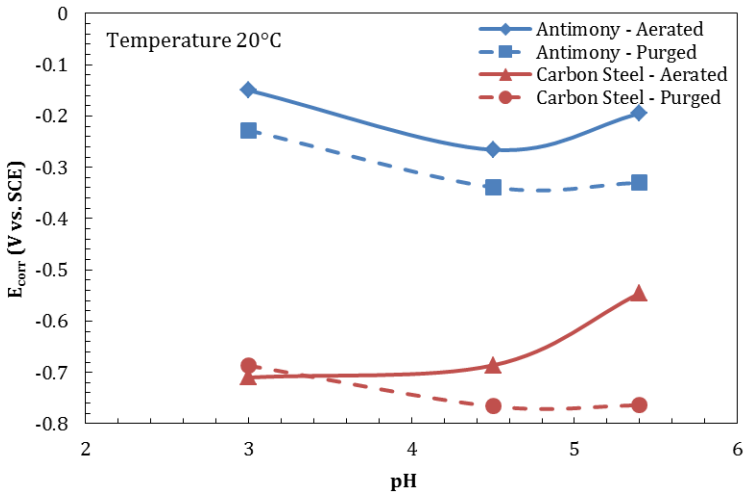

Figure 4: Free corrosion potential, E_{corr} for carbon steel and antimony as a function of pH for the aerated and purged environment at 20°C.

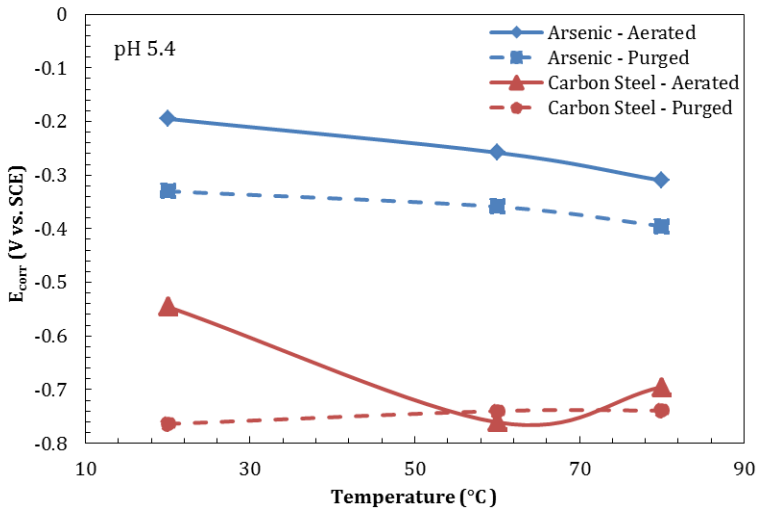

Figure 5: Free corrosion potential, E_{corr} for carbon steel and arsenic (pH 5.4) as a function of temperature for the aerated and purged environment.

3.1.2 Potentiodynamic Polarisation

Corrosion Current Density – Individual Material

Potentiodynamic scans were measured for all materials and Tafel slope analysis was used to calculate the corrosion current. Table 2 gives the calculated corrosion current density (i_{corr}) of all tested materials based on the potentiodynamic polarization measurements. Figure 6 shows the potentiodynamic scans of antimony exposed to pH 3 solution at 20°C and 60°C, with and without aeration. The figure shows increasing corrosion current density with increasing temperature and aeration. The potentiodynamic scans for antimony metal at higher pH values (4.5 and 5.4) also showed an increasing corrosion current density with aeration. A similar trend was observed for arsenic metal and for carbon steel for the same condition.

The results for arsenic were a particular concern as the sintered electrode was expected to have a higher than calculated surface area but the value obtained was in excess of that which might be within acceptable experimental error.

Table 2: Results for i_{corr} for each material taken from the Tafel slopes.

Material	pH	i_{corr} (µA/cm^2)					
		20 °C		60 °C		80 °C	
		Aerated	N_2Purged	Aerated	N_2Purged	Aerated	N_2Purged
Solid Antimony	3	8.13	0.03	223.82	0.21	-	-
	4.5	0.46	0.20	-	-	-	-
Porous Arsenic*	5.4	335.3	1271.7	15.9	3109.8	7845.9	7699.1
Solid Carbon Steel	3	80.79	0.14	479.76	219.93	-	-
	4.5	10.11	0.52	-	-	-	-
	5.4	-	0.14	-	0.13	37.66	9.16

Note: * Expected to be in error due to high surface area of sintered electrode.

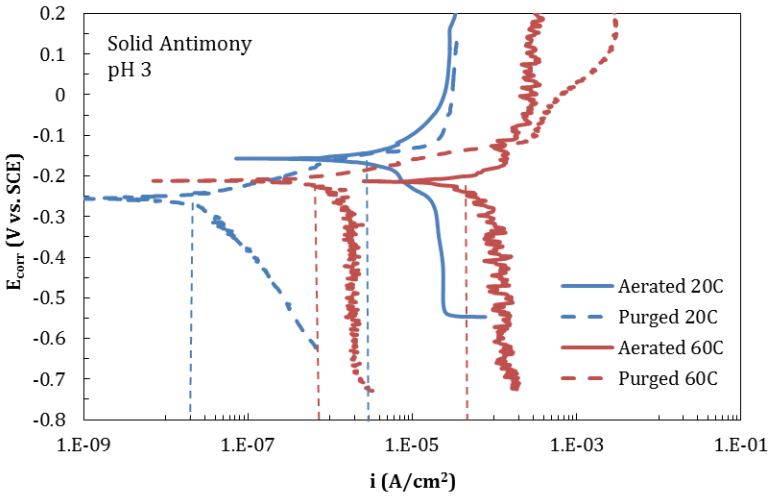

Figure 6: Potentiodynamic curve for solid antimony electrode exposed to aerated and purged environments at pH 3, 20°C and 60°C

Corrosion Current Density – Antimony/Arsenic and Carbon Steel Coupling

Galvanic corrosion current can be roughly predicted by super-imposing polarization curves of the anode and the cathode materials, for example see Figure 7 and Figure 8 for antimony/carbon steel and arsenic/carbon steel couples respectively. The approximate corrosion current densities are summarised in Table 3. The solid antimony to carbon steel super imposing results (Figure 7) were consistent with previously published results [Soltis and Lichti, 2013] and show a significant decrease in coupled current due to purging.

The porous arsenic to carbon steel super imposed results at pH 5.4 and 20°C gave a lower current for aeration than the purged experiment, Figure 8. This again suggests the porous electrode is less than ideal for this work, possibly giving an error in the results due to the high surface area and retained gas (oxygen) within the electrode. In spite of this unexpected result with the porous arsenic electrode, the proposed matrix of electrochemical testing was progressed.

Figure 9 shows how influential the temperature is on the corrosion current of solid antimony in an aerated and a purged environment. In the acidic environment with aeration, increasing the temperature increased the corrosion current. However the same effect was not observed in de-aerated conditions. Figure 10 shows the observed effect of temperature on the corrosion current of the porous arsenic electrode. Both aerated and N_2-purged conditions gave an increase in corrosion rate as temperature was increased. Again, the purged solution had a higher corrosion current than aerated at 20°C.

Table 3: Results for the i_{corr} and corrosion rate for the carbon steel and antimony/arsenic couple.

Material	pH	i_{corr} CR	20°C		60°C		80°C	
			Aerated	Purged	Aerated	Purged	Aerated	Purged
Solid Antimony/CS	3	i_{corr} ($\mu A/cm^2$)	34.10	3.81	145.00	1.89	-	-
		CR (mm/yr)	0.40	0.44	1.69	0.02	-	-
	4.5	i_{corr} ($\mu A/cm^2$)	21.60	1.19	-	-	-	-
		CR (mm/yr)	0.25	0.01	-	-	-	-
	5.4	i_{corr} ($\mu A/cm^2$)	8.5*	2.1*	85*	3.5*	-	-
		CR (mm/yr)	0.10*	0.02*	0.99*	0.04*	-	-
Porous Arsenic/CS	5.4	i_{corr} ($\mu A/cm^2$)	47.9	100.5	293.0	225.0	525.0	382.0
		CR (mm/yr)	0.56	1.17	3.40	2.61	6.10	4.44

Note: *Data from [Soltis and Lichti, 2013]

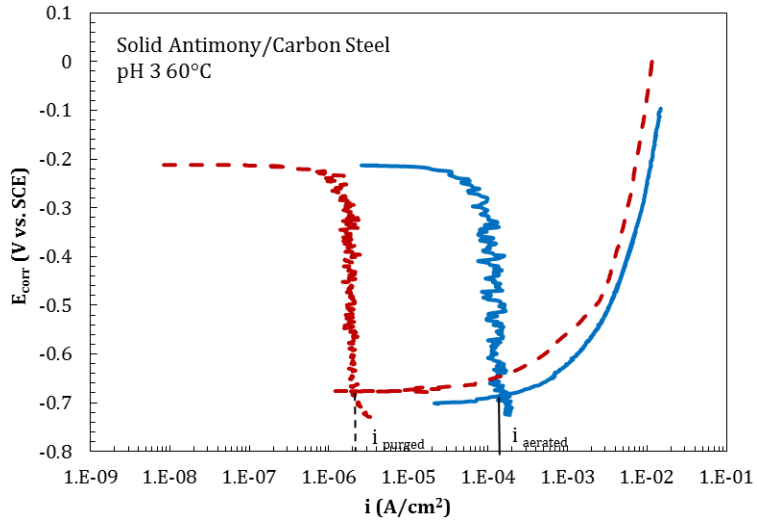

Figure 7: Super-imposed anodic and cathodic curves for carbon steel and solid antimony electrodes exposed to purged environment at pH 3 and 60°C.

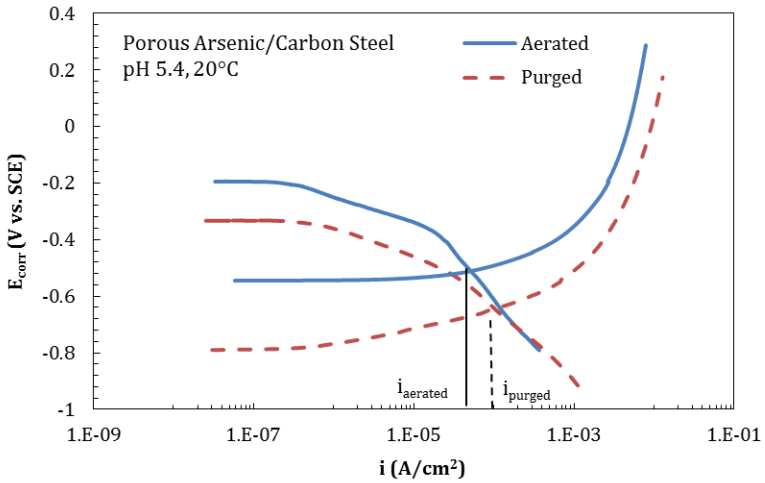

Figure 8: Super-imposed anodic and cathodic curves for carbon steel and porous arsenic electrodes exposed to aerated and purged environment at pH 5.4 and 60°C

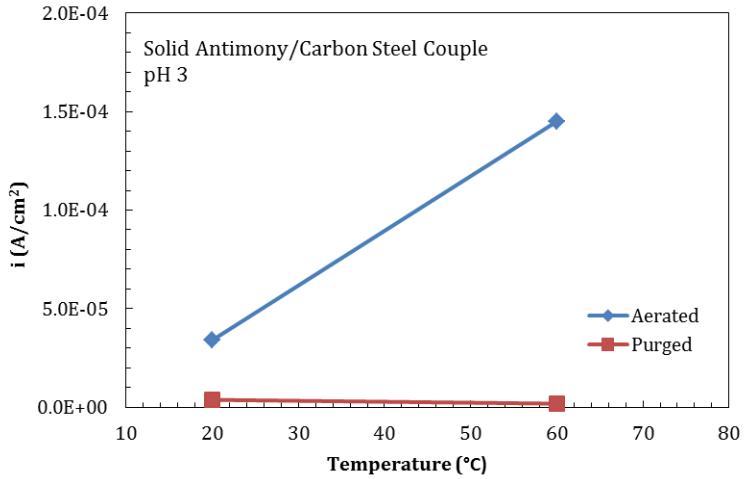

Figure 9: Corrosion current, i_{corr} of solid antimony/carbon steel coupling plotted as a function of temperature for aerated and purged environments, pH 3.

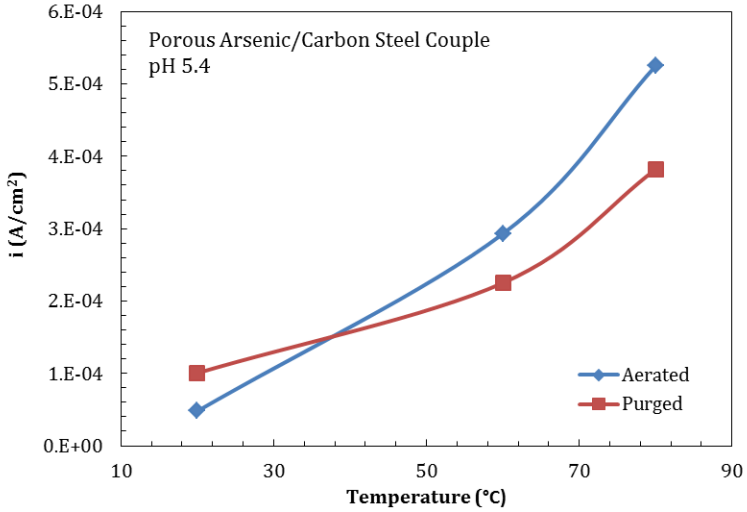

Figure 10: Corrosion current, i_{corr} of porous arsenic/carbon steel coupling plotted as a function of temperature for aerated and purged environments, pH 5.4.

3.1.3 Corrosion Current – Evans Experiments

Evans experiments provide a corrosion current value from the intersection of the working and auxiliary potentials. Table 4 displays the values of the corrosion current obtained in this work. Figure 11 illustrates the results for corrosion current (i_{corr}) of solid antimony and carbon steel in pH 3 and at 20°C under aerated and N_2-purged environments. As expected, the corrosion current of the antimony and carbon steel coupling obtained under aerated condition was higher compared to the N_2-purged condition. At the higher temperature of 60°C, experiments conducted under aerated pH 3 conditions did not produce a mixed potential as the measured potentials of the antimony electrodes were unstable.

Table 4: Results from Evans experiment for the carbon steel-solid antimony and carbon steel –porous arsenic couples.

Material	pH	i_{corr} CR	20 °C		60 °C		80 °C	
			Aerated	Purged	Aerated	Purged	Aerated	Purged
Antimony/CS	3	i_{corr} (µA/cm^2)	37.50	3.55	Unstable	7.69	-	-
		CR (mm/yr)	0.44	0.04	Unstable	0.09	-	-
	4.5	i_{corr} (µA/cm^2)	7.77	2.19	-	-	-	-
		CR (mm/yr)	0.09	0.03	-	-	-	-
	5.4	i_{corr} (µA/cm^2)	7.50*	2.09*	42.20*	4.87*	-	-
		CR (mm/yr)	0.09*	0.02*	0.47*	0.06*	-	-
Arsenic/CS	5.4	i_{corr} (µA/cm^2)	44.59	Unstable	Unstable	Unstable	Unstable	Unstable
		CR (mm/yr)	0.52	Unstable	Unstable	Unstable	Unstable	Unstable

Note: * Data taken from [Soltis and Lichti, 2013]

Figure 12 shows the corrosion current for arsenic in pH 5.4, aerated solution at 20°C. Evans experiments of arsenic and carbon steel coupling conducted under N_2-purged condition and also at higher temperatures were inconclusive. The potential readings for the arsenic electrodes were unstable, possibly due to the porous nature of the arsenic electrode. I_{corr} values between Evans experiments and the super-imposed method were roughly comparable.

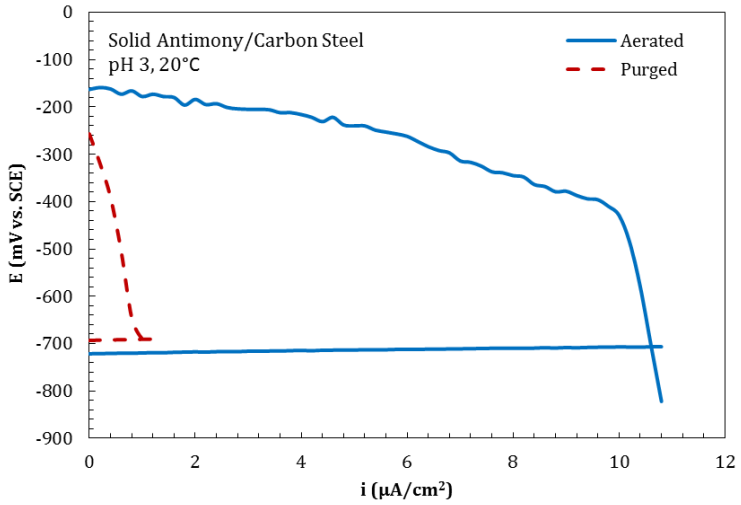

Figure 11. Evans experiment in aerated and purged environment in at pH 3 and 20°C. Intersection of graph indicates i_{corr}.

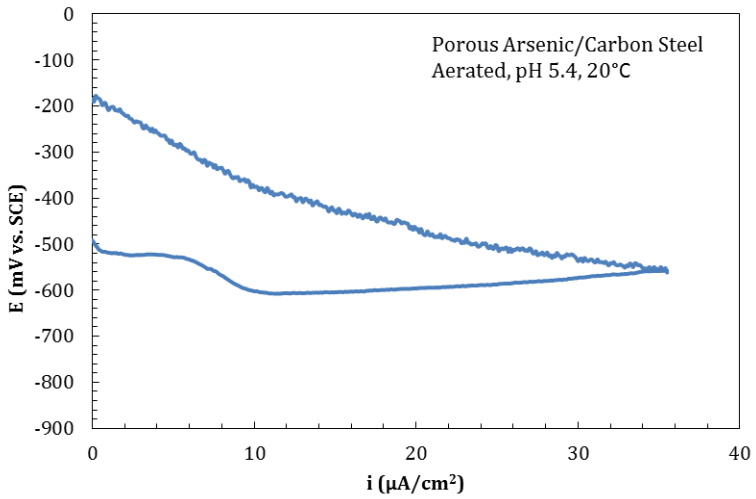

Figure 12: Evans experiment in an aerated environment at pH 5.4 and 20°C. Intersection of graph indicates i_{corr}.

3.2 Coupon Exposure Results

The primary reason for completing coupon exposures was the ability to test densely coated arsenic in contact with carbon steel and to compare this with densely coated antimony in contact with carbon steel. These coated steels were not suitable for electrochemical testing due to difficulties in exposing the fragile coating in the test arrangement. The measurement of free corrosion potential for example will include some contribution from mixed potential of coated metal and the underlying carbon steels. In order to obtain realistic potentials for all tests, the coating was 'scratched' for E_{corr} monitoring.

Figure 13 presents the free corrosion potential (E_{corr}) measurement for "scratched" antimony and arsenic coated carbon steel coupons exposed to aerated pH 5.4 and pH 3 solutions at 20°C. With the exception of antimony coated carbon steel at pH 3, the E_{corr} results indicate that antimony and arsenic metal dominated initially and held the potential more positive, being the larger area and the less electronegative material compared to carbon steel in the galvanic series. After some time a more negative mixed potential, close to that expected for carbon steel in this environment was observed. The free corrosion potential for antimony coated carbon steel exposed to pH 5.4 solution showed instability but followed a similar trend. However, antimony coated carbon steel at pH 3 solution showed a different trend as at the start of the test, E_{corr} was dominated by the carbon steel potential, presumably due to the effect of the strong acid on the antimony layer at the antimony to carbon steel interface.

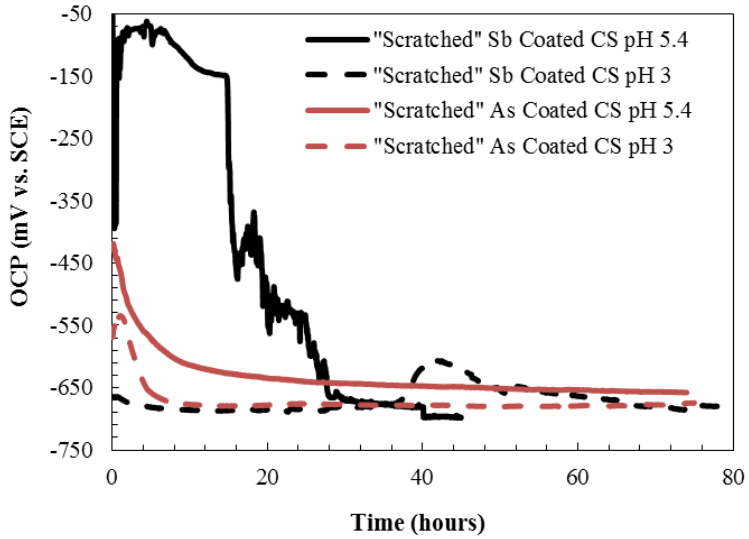

Figure 13: Open circuit monitoring for ''scratched'' antimony and arsenic coated carbon steel at pH 5.4 (Test 1) and pH 3 (Test 2), aerated and at 20°C.

3.2.1 Test 1, pH 5.4 at 20 °C (aerated)

Test one was for arsenic and antimony coated CS coupons exposed to aerated pH 5.4 solution at 20°C. A plain carbon steel coupon was also exposed for comparison. Following the exposure, all of the exposed coupons were partially covered in brown deposit (Figure 14). For the antimony and arsenic coated coupons, areas of spalled/damaged coating were observed on both the scratched and unscratched coupon surfaces. The unscratched coupon had a similar appearance. A brown precipitate formed as a result of dissolved iron leaching from corrosion below the coatings was observed for all coated coupons.

The coupons were subsequently chemically cleaned to reveal the extent of surface corrosion under the deposit. The cleaned antimony coated coupons showed localised corrosion damage near the scratch area as well as at locations away from the scratch area, see Figure 15a and Figure 15b. Similarly, the arsenic coated coupon surface had large areas of removed or spalled coating surrounded by discrete islands of intact coating. Where the coating was absent, the underlying steel surface had an 'etched' appearance, typical of acid attack, and in some instances deep pitting corrosion was observed, see Figure 15c to Figure 15f. It should be noted that some of the areas of the "scratched" surface where carbon steel was exposed remained un-corroded, see Figure 15f.

The pit depths on the coupons were measured and the five deepest pits observed on each of the exposed coupons are reported in Table 5. The scratched antimony coated coupon had a maximum pit depth of 23µm while the unscratched antimony coated coupon had a maximum pit depth of 84µm. The pit depths measured on the arsenic coated coupons were less severe and of the order 35 µm.

The cleaned CS coupon had an 'etched' appearance, typical of acid attack revealing individual grain facets and grain boundaries, Figure 16. Extensive pitting corrosion was observed under the brown deposit with a maximum measured pit depth of 39 µm. In the area free of brown deposit, general corrosion was observed with surface roughness of around 10 µm.

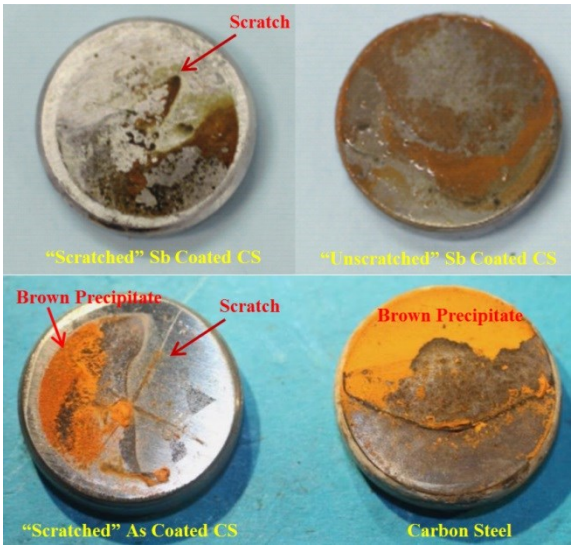

Figure 14: View of at the as-exposed coupons from test 1, conditions: pH 5.4, 20°C, aerated.

a) View of cleaned 'scratched' antimony coated coupon surface showing pitting corrosion next to and on the scratched area, surrounded by retained coating.

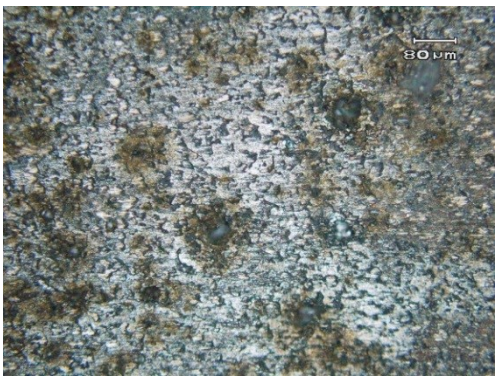

b) View of cleaned 'unscratched' antimony coated coupon surface showing several large pits.

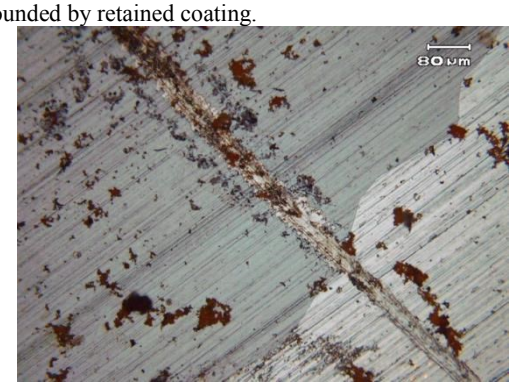

c) As-exposed surface showing non-corroded "scratched" surface and area of spalled coating.

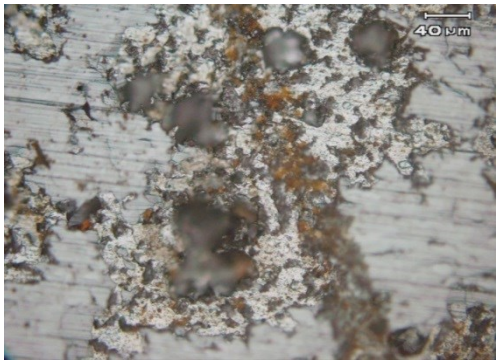

d) View of the coupon after cleaning showing pitting corrosion next to the scratched area surrounded by retained coating areas but not on the scratch.

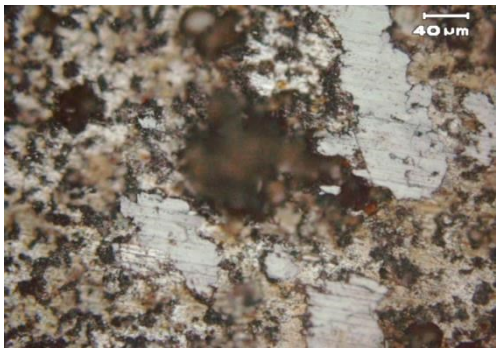

e) View of coupon after cleaning showing pitting under brown area with retained coating areas.

f) View of un-corroded carbon steel surface with pre-existing coating damage.

Figure 15: Optical images "scratched" antimony coated and arsenic coated carbon steel coupons from Test 1, pH 5.4, as-exposed and after clean.

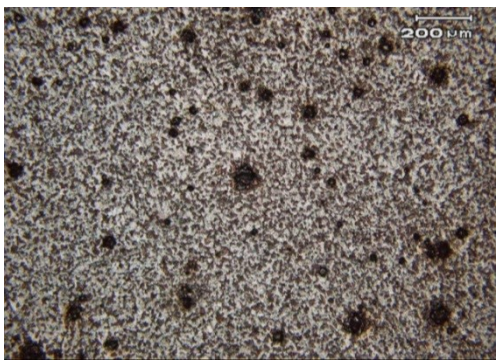

a) Optical image of general surface corrosion and localised pitting corrosion under brown precipitate.

b) Close up view of pitting corrosion and 'etched' general corrosion appearance of carbon steel surface.

Figure 16: Optical images of cleaned carbon steel coupon from Test 1, pH 5.4, 20°C aerated.

Table 5: Pit depth measurement for coupons exposed in Test 1, pH 5.4, 20°C aerated.

Pit	pH 5.4, 20°C, aerated conditions							
	"scratched" Sb coated CS		"unscratched" Sb coated CS		"scratched" As coated CS		CS coupon	
	Depth (µm)	Pitting Rate (mm/yr)	Depth (µm)	Pitting Rate (mm/yr)	Depth (µm)	Pitting Rate (mm/yr)	Depth (µm)	Pitting Rate (mm/yr)
#1	23	2.1	84	7.67	30	2.74	22	2.01
#2	20	1.83	81	7.39	35	3.2	21	1.92
#3	20	1.83	80	7.3	35	3.2	22	2.01
#4	21	1.92	78	7.12	29	2.65	39	3.56
#5	19	1.73	76	6.94	28	2.56	24	2.19
Mean	20.6	1.88	79.8	7.28	31	2.83	25	2.28
Max	23	2.1	84	7.67	35	3.2	39	3.56

3.2.2 Test 2, pH 3 at 20°C (aerated)

Test 2 was for antimony and arsenic coated carbon steel coupons exposed to aerated pH 3 solution at 20°C. A plain carbon steel coupon was also exposed for comparison. All of the exposed coupons had a significant amount of brown precipitate on the surface after testing. The unscratched coupons had brown precipitate that was readily removed by rinsing with distilled water. This brown precipitate indicates that the underlying carbon steel had corroded and damage to the coatings layer had occurred.

Close up views of the cleaned antimony and arsenic coated coupons are shown in Figure 18. Both the antimony and arsenic coated coupons showed large areas of coating breakdown as well as localised coating damage. However, there was no preferential localised corrosion or pitting observed around the scratched areas. The pit depths on the coupons were measured and the five deepest pits observed on each of the exposed coupons are reported in Table 6.

The maximum pit depth measured on the antimony coated coupons was around 83µm. For arsenic coated coupons, the extent of pitting corrosion was again less severe. A pit depth of up to 22 µm was observed within larger areas of damaged coating. Where the coating damage was localised, corrosion of the underlying carbon steel substrate was also observed to a depth of up to 20 µm which added to the total depth of corrosion penetration.

The "un-scratched" arsenic coated coupon which appeared to have maintained an intact coating after exposure in pH 3 solution also showed localised coating loss after the chemical cleaning. This under film corrosion is consistent with the observation of brown precipitate on the coupon surface (*i.e.* corrosion of iron and iron transport through defects in the coating). The cleaned un-scratched arsenic coated coupon surface had random areas of large coating loss. Where large areas of coating were lost, shallow pitting and general surface corrosion of the carbon steel substrate were observed. However, in areas where the coating damage was isolated, pitting corrosion to depth of up to 37 µm was observed (Figure 18f).

Views of the cleaned carbon steel coupon surface are given in Figure 19. The corroded carbon steel surface had an 'etched' appearance with surface roughness of around 6 to 8 µm. No deep corrosion pitting was observed on the carbon steel coupon. The testing at pH 3 with aeration gave a maximum rate of attack of 7.6 mm/year and 3.4 mm/year for the antimony and arsenic coated carbon steel respectively, in contrast to the maximum rate of attack of 0.73 mm/year on the uncoated carbon steel.

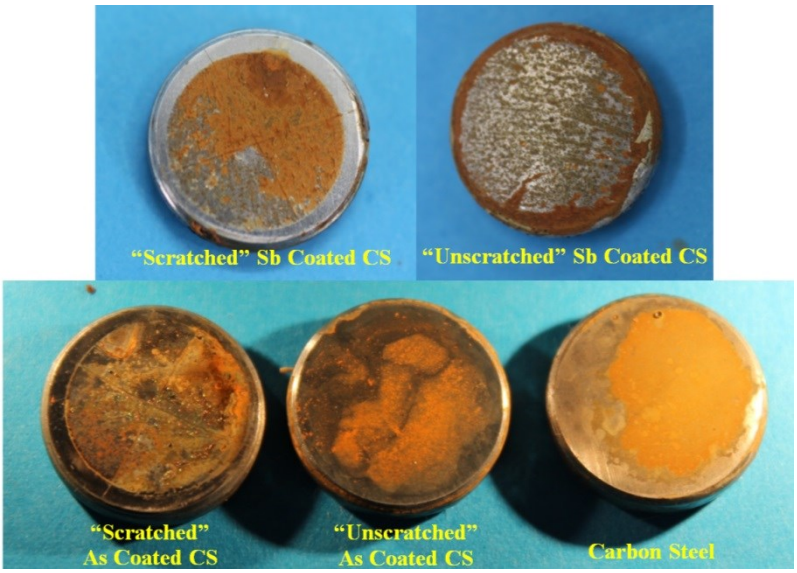

Figure 17: View of at the as-exposed coupons from Test 2, conditions: pH 3, 20°C, aerated.

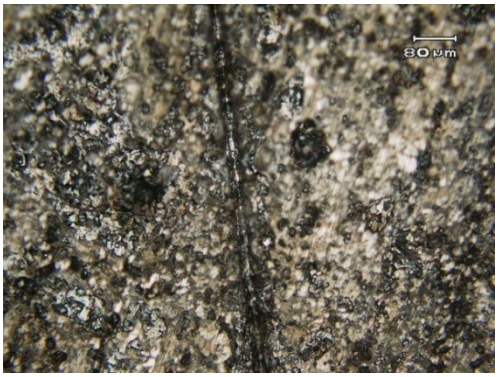

a) View of cleaned 'scratched' antimony coated coupon surface showing pitting next to the scratch.

b) View of cleaned 'unscratched' antimony coated coupon surface showing pitting next to the scratch.

c) Close up view of as-exposed surface of "scratched" arsenic coated coupon showing coating spalling.

d) View of cleaned arsenic coated coupon near the scratched area showing pitting corrosion within area of damaged coating. Note the 'etched' appearance of the carbon steel.

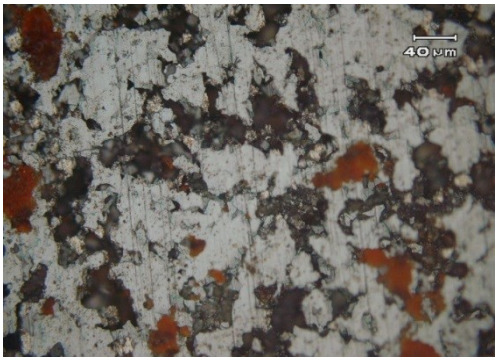

e) View of cleaned arsenic coated coupon away from the scratched area showing localised corrosion and retained areas of coating.

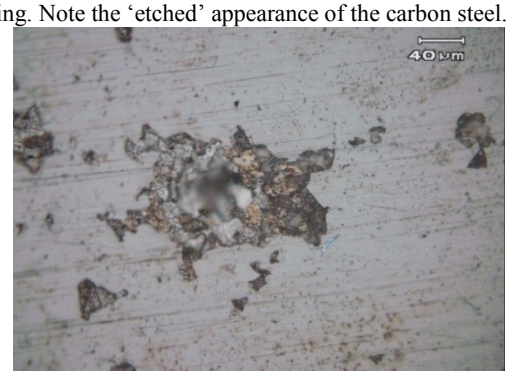

f) "Unscratched" arsenic coated coupon surface showing isolated deep pit within small area of damaged coating.

Figure 18: Optical images antimony coated and arsenic coated with carbon steel couple from test 2, pH 3 as-exposed and after clean.

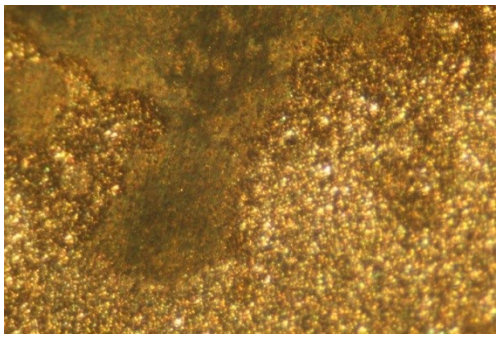

a) Close up view of cleaned carbon steel.

b) View of the cleaned carbon steel coupon showing roughened and 'etched' surface.

Figure 19: Views of CS coupon from Test 2, pH 3, 20°C aerated solution after cleaning.

Table 6: Pit depth measurement for coupons exposed in Test 2, pH 3, 20°C aerated.

Pit	pH 3, 20°C, aerated condition									
	"scratched" Sb coated CS		"unscratched" Sb coated CS		"scratched" As coated CS		"unscratched" As coated CS		CS coupon	
	Depth (µm)	Pitting Rate (mm/yr)	Depth (µm)	Pitting Rate (mm/yr)	Depth (µm)	Pitting Rate (mm/yr)	Depth (µm)	Pitting Rate (mm/yr)	Depth (µm)	Pitting Rate (mm/yr)
#1	75	6.84	66	6.02	22	2.01	25	2.28	6	0.55
#2	39	3.56	36	3.29	17	1.55	19	1.73	6	0.55
#3	77	7.03	51	4.65	15	1.37	17	1.55	8	0.73
#4	83	7.57	34	3.1	13	1.19	10	0.91	6	0.55
#5	81	7.39	32	2.92	20	1.83	37	3.38	6	0.55
Mean	71	6.4	43.8	4	17	1.55	23	2.1	7	0.64
Max	83	7.57	66	6.02	22	2.01	37	3.38	8	0.73

3.2.2 Cross Sectional Analysis

Selected coupons were sectioned and mounted in resin for cross sectional analysis. The samples were then ground and polish to 1 micron surface finish for detailed analysis using optical microscopy, scanning electron microscopy (SEM) and energy dispersive spectroscopy (EDX). SEM images are shown using back scatter technique to show different contrast between areas with different chemical compositions (heavier elements will appear brighter in the image).

A profile of pitting corrosion found on the antimony coated coupon exposed to aerated pH 5.4 solution is shown in Figure 20. The SEM-EDX analyses results for this cross section are shown in Table 7. Carbon was not included as the results were unreliable. Figure 20 shows more or less intact antimony coating on the coupon surface, over the pit area (indicated by the bright layer, Spot 3 in Table 7). The pit contained small amount of corrosion product that were rich in iron and oxygen, indicating presence of iron oxide compounds. Low levels of chlorine were detected in all analysis.

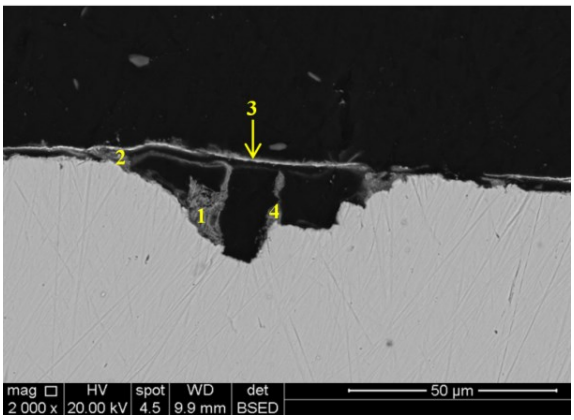

Figure 20: SEM image of a pit on 'scratched' antimony coated coupon exposed to aerated pH 5.4 solution.

Table 7: SEM-EDX analysis of pit area shown in Figure 20.

Location		O	Cl	Sb	Fe	Si
Spot 1	Wt. %	13.57	1.28	2.96	82.19	-
	At. %	35.64	1.52	1.02	61.82	-
Spot 2	Wt. %	11.54	1.15	39.16	43.3	4.85
	At. %	35.65	1.6	15.9	38.32	8.53
Spot 3	Wt. %	15.55	2.38	53.55	28.52	-
	At. %	48.84	3.38	22.11	25.67	-
Spot 4	Wt. %	14.86	1.77	-	83.37	-
	At. %	37.59	2.02	-	60.4	-

4. SUMMARY OF CARBON STEEL – HEAVY METAL COUPLES

4.1 Electrochemical Testing

The electrochemical testing with the solid antimony and carbon steel super-imposed and solid antimony to carbon steel couples showed increasing carbon steel corrosion for coupled materials as: aeration is added, pH is decreased and temperature is increased.

Reduction in pH had only minor effect on corrosion rate under nitrogen purged conditions up to the test temperature of 60°C. The porosity of the arsenic electrode gave unexpected high corrosion currents when coupled to carbon steel. The results obtained are considered unreliable.

4.2 Coated Coupon Testing

All of the carbon steel-heavy metal couple testing to date has been done at 20°C and all with aerated solutions. The results were definitive in showing that the corrosion under the antimony layer coating was always greater than on uncoated steel and greater than on steel exposed by scratching the arsenic layer. The work suggests that the main mechanism of corrosion is one of chloride pitting under a cathodic surface layer. By implication this corrosion must have initiated at defects in the antimony and arsenic coating. In combination, the cross section results suggest a model for the carbon steel corrosion under layers of reductively deposited heavy metal scales being mainly due to chloride induced pitting corrosion. The heavy metal coatings provide a stable large area anode external to the corroding pit. Initiation is easily facilitated though defects in the heavy metal deposit.

The use of the aerated fluids provided a means of readily observing differences on the exposed couples as aeration strongly accelerated the galvanic corrosion and the pitting corrosion as demonstrated by the electrochemical testing. A more rigorous experimental programme and analysis will be required for future work as the clear distinction of pitting *vs.* no pitting and galvanic acceleration *vs*. no acceleration may not occur for non-aerated environments at these same temperatures. However, at lower pH even the de-aerated environments would be expected to show good differentiation for effects of pH and temperature.

5. FUTURE WORK

The high carbon steel electrode to porous arsenic electrode current density is believed to indicate that with an increased surface area of arsenic the galvanic corrosion of the carbon steel is significantly enhanced. Effort is still required to obtain solid arsenic electrode suitable for electrochemical studies. Future work will include not only attempts to prepare a solid arsenic electrode but also to complete further electrochemical testing that shows the effect of large area ratios of antimony and arsenic to carbon steel. Although the coupon tests suggest some effect electrochemical testing would better quantify the effect of the area ratio parameter. The coupon exposure results suggest galvanic corrosion is less severe with arsenic overlaying carbon steel compared to antimony overlaying carbon steel. This method of test is more difficult than the electrochemical testing but does give reliable results. Further work is required to validate the obtained results and to extend the test matrix to environments of higher temperature and added gasses CO_2 and H_2S.

6. ACKNOWLEDGEMENT

This paper was prepared with the support of Quest Integrity NZL Ltd and GNS Science, New Zealand, Core Science Area, Geothermal Research Program (previously from the Foundation for Research Science and Technology (FRST) PROJ-12405-IFS “Geothermal: New Zealand's Energy Solution”). We thank Dr. Vivian Fang for the technical assistance to prepare the ion beam sputter coating.

REFERENCES

Amend, B. and Yee, J. : Selective Application of Corrosion Resistant Alloys Mitigates Corrosion in pH-Modified Geothermal Fluids, *Proceedings* NACE Corrosion 2013, Paper No C2013-0002416 (2013).

Gallup, L., Featherstone, J. L., Reverente, J. P., and Messer, P. H. : Line Mine: A Process For Mitigating Injection Well Damage At The Salton Sea, California (USA) Geothermal Field, WGC, Italy, pp 2403-2408 (1995).

Lichti, K. A. and Brown, K. L. : Prediction and Monitoring of Scaling and Corrosion in pH Adjusted Geothermal Brine Solutions, *Proceedings* NACE Corrosion 2013, Paper No C2013-0002544 (2013).

Lichti, K. A.: Forgotten Phenomenon of Materials Selection and Use in Geothermal Energy Applications, Published in Materials Issues Governing the Performance of Advanced 21st Century Energy Systems, Wellington New Zealand, February-March 2006, *Science Reviews*. 2007, Science Reviews 2000 Ltd, pp 243-255.

Murmu, P., Kennedy, J.V**.**, Ruck, B.J., Markwitz, A.: Characterization of the structural and electrical properties of ion beam sputtered ZnO films, *Materials science forum* 700. pp 49-52 (2011).

Shannon, D. W. : Corrosion of Iron-Base Alloys Versus Alternate Materials in Geothermal Brines, Interim Report October 1977, Battelle Pacific Northwest Laboratories, Richland, Washington (USA) (1977).

Soltis, J. and Lichti, K. A. : Galvanic Corrosion of Carbon Steel Coupled to Antimony, *Corrosion Science*, **68**, (2013), 162–167.